



**Paraffinic metal–organic polyhedrons: Solution-processable porous modules exhibiting three-dimensional molecular order**

Journal:	<i>ChemComm</i>
Manuscript ID	CC-COM-05-2018-003705.R1
Article Type:	Communication

SCHOLARONE™  
Manuscripts



## Paraffinic metal–organic polyhedrons: Solution-processable porous modules exhibiting three-dimensional molecular order

Received 00th January 20xx,  
Accepted 00th January 20xx

Kenichiro Omoto, Nobuhiko Hosono,\* Mika Gochomori and Susumu Kitagawa\*

DOI: 10.1039/x0xx00000x

www.rsc.org/

**Metal–organic polyhedral cages substituted with paraffinic side chains were designed as solution-processable porous modules, which provide soft materials possessing self-organized cavity structures with three-dimensional molecular order in a lyotropic mesophase. The macroscopic shape of the resulting soft materials can be easily modified through solution-based processes.**

Porous crystalline materials are attractive for their potential functionalities such as molecular separation,<sup>1</sup> storage,<sup>2</sup> transportation,<sup>3</sup> recognition,<sup>4</sup> and guest ordering<sup>5</sup> in confined spaces. The regular three-dimensional order of discrete nanocavities is an essential feature for such porous materials that are generally recognized as hard and fragile matters. Porous coordination polymers (PCPs) and metal–organic frameworks (MOFs) are emerging as porous crystalline materials that offer high degrees of designability for framework and pore structures.<sup>6</sup> Typically, the pore sizes and dimensions, as well as the chemical interaction sites (e.g., open-metal sites), can be designed in a rational manner using an appropriate isorecticular approach and/or metal selection/ligand design. Although PCPs/MOFs appear to be promising porous materials for the aforementioned functionalities, their low processability due to the crystalline nature remains a formidable challenge and manufacturing practical forms, such as uniform membranes, films, and pellets, is a difficult task that needs to be addressed.

Recently, some PCPs/MOFs that show melting behavior, thus forming an amorphous/liquid phase, have been discovered.<sup>7</sup> In this melting event, the long-range molecular ordering in the framework is lost, while the primary coordination networks and chemical configurations of original PCPs/MOFs are retained. Although this melting approach could offer a potential top-down route to access processable porous

materials, the well-defined structures of cavities with long-range molecular order are sacrificed by melting into a glassy state. Hence, a conceptual breakthrough for the synthesis of processable PCP/MOFs that preserve the discrete cavities and long-range ordering is required. The development of truly processable PCP/MOF analogues would lead to mendable and self-healing PCPs/MOFs that are in demand for diverse future applications.

In a different approach, fluidic porous materials have been recently proposed and synthesized using organic cage molecules, which suggests that cage-type compounds are potential discrete nanocavity modules.<sup>8</sup> On the other hand, liquid-crystalline (LC) materials and LC polymer networks,<sup>9–11</sup> which exhibit both nanoporosities and highly ordered structures on a macroscopic scale, have been synthesized so far and demonstrated to have potential as molecular separation membranes. These interdisciplinary examples prompted us to develop a new paradigm for processable PCP/MOF-based materials using a bottom-up approach to address the above-mentioned issues.

Herein, we propose bottom-up modular synthesis of LC porous materials consisting of metal–organic polyhedrons (MOPs)<sup>12,13</sup> as cavity modules that organize into a lyotropic LC phase. Cage modules functionalized with alkyl chains can self-organize into a body-centered cubic (bcc) ordered structure in the presence of solvent molecules. The fluidic features of the LC phase afford high processability, allowing various forms, including films, to be obtained with regular arrangements of nanocavities.

MOPs are a class of discrete cage-type PCP/MOF analogues that are self-assembled from multiple ditopic bent ligands and metal ions.<sup>12–14</sup> MOPs generally adopt a spherical shape with a nanometer-sized void core that can accommodate a variety of small molecules. The peripheral surface of MOPs can be easily functionalized with molecular or polymeric substituents at the convex position of the ligand, which allows tuning of the intermolecular interactions of MOPs and the packing structures, thus controlling the self-organizing behavior.<sup>14</sup> In this study, we used a representative cuboctahedral MOP,

<sup>a</sup> Institute for Integrated Cell-Material Sciences (WPI-iCeMS), Kyoto University Institute for Advanced Study (KUIAS), Kyoto University, Yoshida Ushinomiya-cho, Sakyo-ku, Kyoto 606-8501, Japan. E-mail: nhosono@icems.kyoto-u.ac.jp; kitagawa@icems.kyoto-u.ac.jp

Electronic Supplementary Information (ESI) available: Experimental details including syntheses and X-ray scattering analyses. See DOI: 10.1039/x0xx00000x

$\text{Cu}_{24}\text{Ip}_{24}$ , composed of 24 isophthalate ( $\text{Ip}^{2-}$ ) groups interconnected with 12 dicopper paddlewheel clusters, as a porous core module.<sup>13</sup> The complexation reaction between  $\text{Ip}^{2-}$  and  $\text{Cu}^{\text{II}}$  instantly yields a cuboctahedral MOP with an external diameter of  $\sim 2.4$  nm (Fig. 1a). The MOP core itself without any solubilizing functional groups provides an insoluble agglomerated material owing to strong inter-MOP interactions and less solvation property because of the large molecular size.

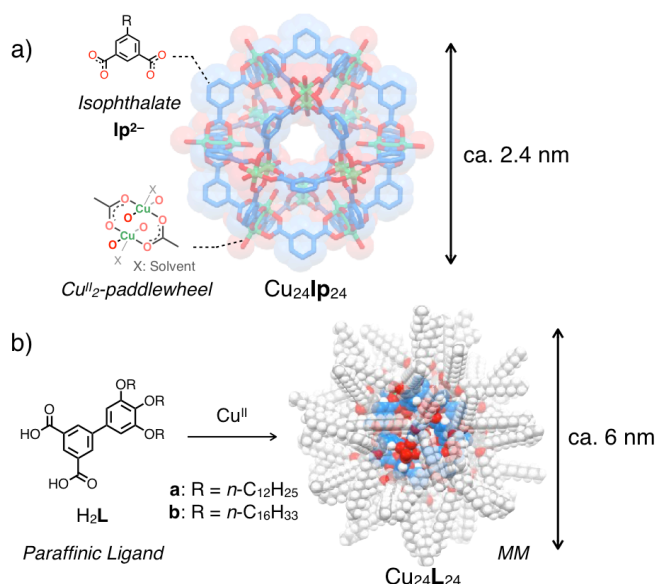
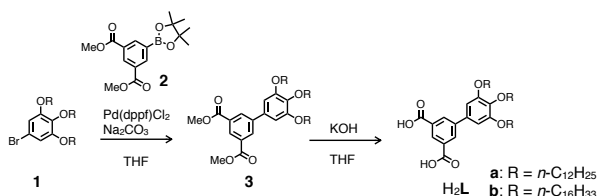


**Fig. 1.** a) Core structure of a homoleptic cuboctahedral MOP ( $\text{Cu}_{24}\text{IpR}_{24}$ ). b) Scheme for the formation of paraffinic MOP  $\text{Cu}_{24}\text{LR}_{24}$  through coordination-driven self-assembly of the paraffinic ligand  $\text{H}_2\text{L}$  and  $\text{Cu}^{\text{II}}$ . The C atoms of the isophthalate moieties are colored blue.

To reduce the inter-MOP interactions, we designed paraffinic isophthalate ligands,  $\text{H}_2\text{La}$  and  $\text{H}_2\text{Lb}$ , which possess three *n*-dodecyloxy (*n*- $\text{C}_{12}\text{H}_{25}$ ) and *n*-hexadecyloxy (*n*- $\text{C}_{16}\text{H}_{33}$ ) groups, respectively, as lubricating side chains (Fig. 1b). Each ligand was prepared and isolated as a colorless solid via a Pd-catalyzed coupling reaction between 5-bromo-1,2,3-tris-(alkoxy)-benzene (**1**) and dimethyl-5-(4,4,5,5-tetramethyl-1,3,2-dioxaborolan-2-yl)isophthalate (**2**), followed by hydrolysis of the diester (**3**) under basic conditions (Scheme 1, ESI).



**Scheme 1.** Syntheses of paraffinic ligands.

We examined the MOP formation reaction of the paraffinic ligand  $\text{H}_2\text{La}$  in the presence of  $\text{Cu}(\text{OAc})_2 \cdot \text{H}_2\text{O}$  (Fig. 2a). We used slightly excess amount of  $\text{Cu}(\text{OAc})_2 \cdot \text{H}_2\text{O}$ , ca. 1.3 equiv. to the ligand, in order to ensure a completion of the reaction. The 5-*tert*-butylisophthalic acid ligand ( $\text{H}_2\text{IptBu}$ ) was also tested for comparison. As previously reported, a 1:1 mixture of  $\text{H}_2\text{IptBu}$  and  $\text{Cu}(\text{OAc})_2 \cdot \text{H}_2\text{O}$  in *N,N*-diethylformamide (DEF) yields a cuboctahedral MOP architecture, namely,  $\text{Cu}_{24}\text{IptBu}_{24}$  (Fig. 2c).<sup>13b</sup> A single crystal of  $\text{Cu}_{24}\text{IptBu}_{24}$  MOP, synthesized according to the literature procedure, was dissolved in THF and subjected to size-exclusion chromatography (SEC). In SEC,  $\text{Cu}_{24}\text{IptBu}_{24}$  was clearly detected as a monodisperse peak ( $t = 17.2$  min) at a shorter elution time than that of the ligand,  $\text{H}_2\text{IptBu}$  ( $t = 19.9$  min; Fig. 2c).<sup>14d</sup> Similarly, a 1:1.3 mixture of  $\text{H}_2\text{La}$  and  $\text{Cu}(\text{OAc})_2 \cdot \text{H}_2\text{O}$  in THF gave a monodisperse peak in SEC ( $t = 15.8$  min; Fig. 2b) at a shorter elution time than  $\text{H}_2\text{La}$  ( $t = 18.5$  min), indicating the formation of the corresponding MOP, namely  $\text{Cu}_{24}\text{La}_{24}$  (hereafter termed **MOP-a**), as a discrete and stable product under this condition. The elution time of **MOP-a** was much shorter than that of  $\text{Cu}_{24}\text{IptBu}_{24}$ , which suggests that **MOP-a** has a larger hydrodynamic volume than the reference MOP owing to multiple alkyl side chains covering the surface of its polyhedral cage core.

The formation of **MOP-a** was also supported by matrix-assisted laser desorption/ionization time-of-flight (MALDI-TOF) mass spectrometry, which showed a prominent peak at  $m/z = 20568.94$  corresponding to the molecular weight of an ionized **MOP-a** species (calculated molecular weight of **MOP-a**: 20561.50 Da; Fig. 3). The resulting complex was readily isolated as a blue viscous material by precipitation using MeOH as a poor solvent (ESI).

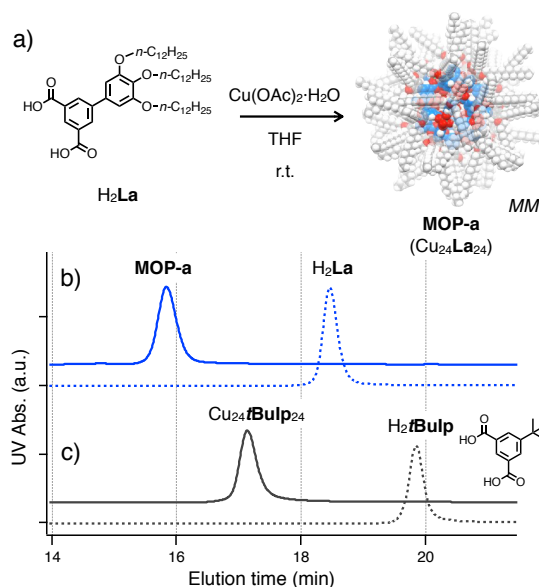


**Fig. 2.** a) Synthesis of **MOP-a** ( $\text{Cu}_{24}\text{La}_{24}$ ). SEC traces of b) **MOP-a** prepared from a 1:1.3 mixture of  $\text{H}_2\text{La}$  and  $\text{Cu}(\text{OAc})_2 \cdot \text{H}_2\text{O}$  in THF (upper, blue solid line),  $\text{H}_2\text{La}$  (lower, blue dotted line), c)  $\text{Cu}_{24}\text{IptBu}_{24}$  prepared from a 1:1 mixture of  $\text{H}_2\text{IptBu}$  and  $\text{Cu}(\text{OAc})_2 \cdot \text{H}_2\text{O}$  in DEF (upper, black solid line), and  $\text{H}_2\text{IptBu}$

(lower, black dotted line). SEC chromatograms were recorded at 313 K with a UV detector using THF as the eluent.

In a similar manner, **MOP-b** ( $\text{Cu}_{24}\text{Lb}_{24}$ ), possessing *n*-hexadecyloxy side-chains, was prepared by  $\text{Cu}^{\text{II}}$ -complexation using  $\text{H}_2\text{Lb}$  as a paraffinic ligand. **MOP-b** was isolated as a blue viscous material and characterized by SEC and MALDI-TOF mass spectrometry (ESI). The monodisperse SEC peak of **MOP-b** appeared at a slightly shorter elution time ( $t = 15.7$  min) than **MOP-a**, reflecting the much longer alkyl side chains attached to the MOP surface. The external diameters of **MOP-a** and **MOP-b** were calculated by molecular mechanics (MM) modeling as ca. 6 nm and ca. 7 nm, respectively. It should be noted that both **MOP-a** and **MOP-b** are highly soluble in typical organic solvents such as *n*-hexane,  $\text{Et}_2\text{O}$ ,  $\text{CHCl}_3$ ,  $\text{CH}_2\text{Cl}_2$ ,  $\text{EtOAc}$ , and THF; however, they are hardly soluble in highly polar solvents such as *N,N*-dimethylacetamide (DMA), DEF, and dimethylsulfoxide (DMSO).

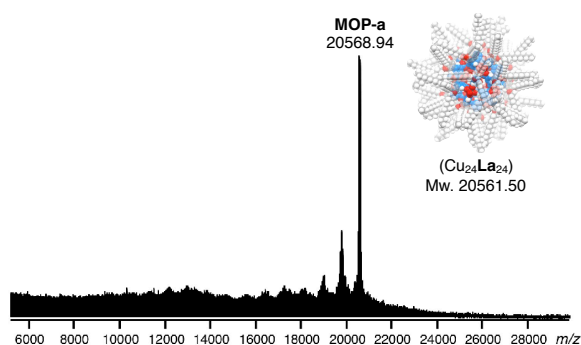


**Fig. 3.** MALDI-TOF mass spectrum (negative) of **MOP-a** (matrix: DCTB).

X-ray diffraction (XRD) measurements were conducted to gain insight into the nanostructures of the paraffinic MOPs. As-prepared samples of **MOP-a** and **MOP-b**, which were isolated as blue viscous materials by precipitation from MeOH and vacuum drying, formed random arrangements without long-range order, as indicated by the appearance of a single broad peak around  $q = 1.70 \text{ nm}^{-1}$  and  $q = 1.55 \text{ nm}^{-1}$ , respectively, at room temperature (Fig. S12, ESI).<sup>14d</sup>

Interestingly, both **MOP-a** and **MOP-b** formed three-dimensional ordered structures upon impregnation with DMA as a dopant (hereafter **MOP-a**<sub>DMA</sub> and **MOP-b**<sub>DMA</sub>, respectively). The XRD data of **MOP-a**<sub>DMA</sub> at 313 K included many sharp diffraction peaks (Fig. 4a). These diffraction peaks were successfully indexed to a bcc structure with a lattice constant of  $a = 4.5 \text{ nm}$ , suggesting the formation of a lyotropic mesophase (Fig. 4b). The cell-diagonal distance of the cubic lattice was calculated as 7.8 nm, from which the distance between MOP cores can be estimated as 3.9 nm. This value is quite small compared with the calculated diameter of **MOP-a** (ca. 6 nm), which implies that ordering of adjacent MOPs involves interdigitation and/or bending of alkyl side chains. For **MOP-a**<sub>DMA</sub>, the content of DMA dopant was ca. 50 wt.%. Only

a small amount of DMA was required to form the ordered structure, but upon removal of DMA by heating, the original bcc structure reorganized into an uncharacterized crystalline structure that exhibited many X-ray diffraction peaks (Fig. S14b, ESI).

Notably, similar self-organization of MOPs into a bcc structure was also observed for **MOP-b** with DMA as the dopant. The bcc lattice constant of **MOP-b**<sub>DMA</sub> was determined as  $a = 4.7 \text{ nm}$ , which is slightly greater than that of **MOP-a**<sub>DMA</sub> owing to its longer alkyl side chains (Fig. S13, ESI).<sup>14d</sup>

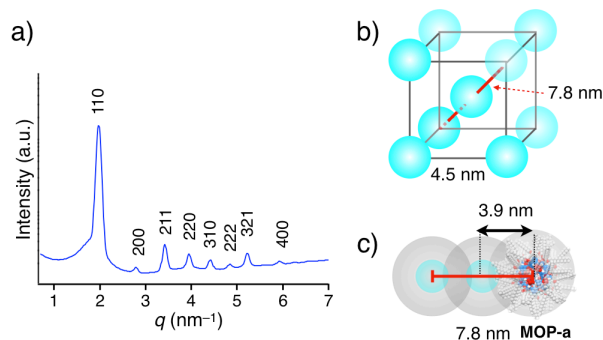


**Fig. 4.** a) XRD profile of **MOP-a**<sub>DMA</sub> at 313 K. The values on the peaks are the Miller indices. b) Postulated body-centered cubic packing of **MOP-a**<sub>DMA</sub> based on the XRD profile in Fig. 4a, and c) the arrangement of MOPs on the cell diagonal at 313 K.

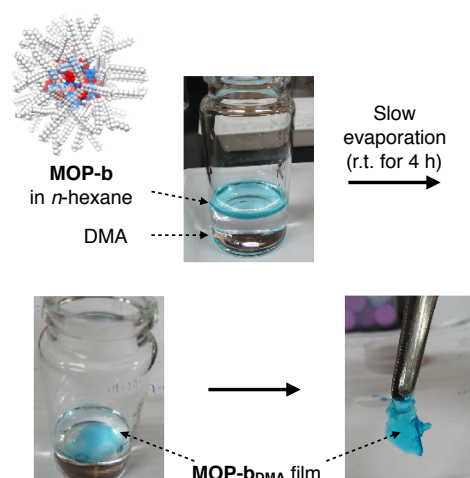


**Fig. 5.** Preparation of a liquid-crystalline film of **MOP-b**<sub>DMA</sub> via a solution-based process.

Unlike common supramolecular cage complexes, **MOP-a** and **MOP-b** are highly soluble in less-polar organic solvents such as *n*-hexane. The solution-processable nature of the paraffinic MOPs prompted us to prepare uniform self-standing films with well-organized arrangements of nanocavities via a solution-based procedure (Fig. 5). An *n*-hexane solution of **MOP-b** was layered on DMA, and the sample was slowly dried at room temperature for 4 h to obtain a blue-colored film that was robust enough to be picked up with tweezers (Fig. 5). The X-ray diffraction pattern of the resulting film was identical to

that of **MOP-b**<sub>DMA</sub>, suggesting that **MOP-b** formed a bcc-type regular ordered structure, even in the film state (Fig. S15, ESI). This result demonstrated the high processability of the MOP-based LC materials, which can be shaped into various practical forms via solution processes.

Thermogravimetric analysis (TGA) and differential scanning calorimetry (DSC) provided us with general thermal properties of MOPs. TGA indicated that **MOP-a** and **MOP-b** without DMA are stable up to 573 K (300 °C) in terms of the weight loss (Fig. S16, ESI). The DSC profile of **MOP-a**<sub>DMA</sub> showed an exothermic peak at 323 K upon cooling that may correspond to a LC phase transition while no significant peak was observed for **MOP-a** in the range of 223 K to 423 K (Fig. S17). This suggests that DMA plays an important role for the structuring of **MOP-a** (See ESI).

In summary, we demonstrated a modular approach for the syntheses of porous LC materials using a metal–organic cage complex as a cavity core module that self-organizes into a three-dimensionally ordered structure. Discrete MOP cages substituted with multiple paraffinic side chains, namely paraffinic MOP cages, were readily synthesized by the self-assembly of Cu<sup>II</sup> ions and paraffinic isophthalates. These MOPs formed a lyotropic LC phase in the presence of DMA as a dopant to provide a soft and fluidic porous material with an ordered bcc packing structure. Moreover, the solution-processability of those MOPs facilitated the fabrication of freestanding films without loss of the ordered structure. The solution-processable and self-organizing nature of paraffinic MOPs offers a new design principle to shape porous materials into films; this approach is expected to be applicable to mass transport and molecular separation media with well-designed nanochannels. However, the present porous LC modules only exhibit an ordered structure in the lyotropic mesophase, which would be a drawback for future versatile applications. Further work is underway to extend this design principle to thermotropic porous LC systems.

This work was supported by a KAKENHI Grant-in-Aid for Specially Promoted Research (JP25000007) from the Japan Society for the Promotion of Science (JSPS). N.H. acknowledges JSPS for KAKENHI Grant-in-Aid for Young Scientists (B) (JP16K17959) and Scientific Research (B) (JP18H02072). S.K. acknowledges the ACCEL program (JPMJAC1302) of the Japan Science and Technology Agency for financial support. The synchrotron radiation (SR) XRD experiments were conducted on BL8S3 at Aichi Synchrotron Radiation Center, Aichi Science & Technology Foundation, Aichi, Japan (Proposal No. 201705044) and BL45XU at SPring-8 with the approval of the Japan Synchrotron Radiation Research Institute (JASRI) (Proposal No. 2016B1264).

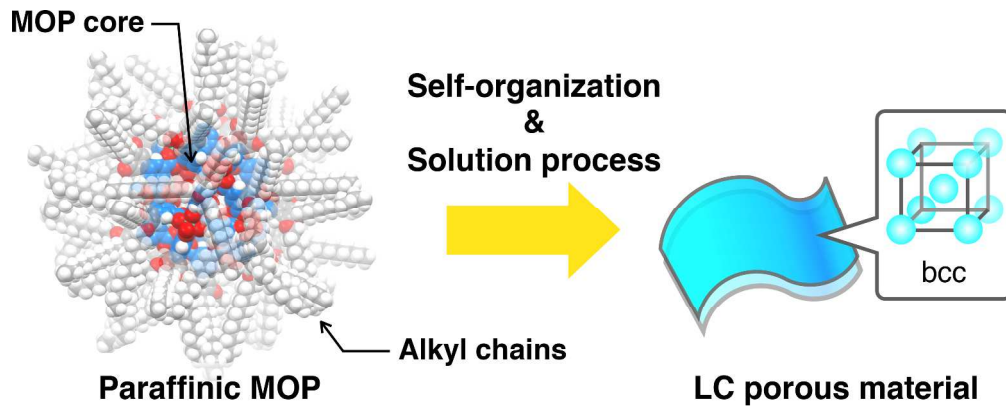
## Conflicts of interest

There are no conflicts to declare.

## Notes and references

- (a) B. Li, H.-M. Wen, W. Zhou and B. Chen, *J. Phys. Chem. Lett.*, 2014, **5**, 3468–3479; (b) K. Adil, Y. Belmabkhout, R. S. Pillai, A. Cadiau, P. M. Bhatt, A. H. Assen, G. Maurin and M. Eddaoudi, *Chem. Soc. Rev.*, 2017, **46**, 3402–3430.
- (a) S. Ma and H.-C. Zhou, *Chem. Commun.*, 2010, **46**, 44–53; (b) Y. He, B. Li, M. O’Keeffe and B. Chen, *Chem. Soc. Rev.*, 2014, **43**, 5618–5656;
- (c) M. F. de Lange, K. J. F. M. Verouden, T. J. H. Vlught, J. Gascon and F. Kapteijn, *Chem. Rev.*, 2015, **115**, 12205–12250.
- (a) S. Horike, D. Umeyama and S. Kitagawa, *Acc. Chem. Res.*, 2013, **46**, 2376–2384; (b) K. Fujie and H. Kitagawa, *Coord. Chem. Rev.*, 2016, **307**, 382–390.
- (a) A. Karmakar, P. Samanta, A. V. Desai and S. K. Ghosh, *Acc. Chem. Res.*, 2017, **50**, 2457–2469; (b) Y. Takashima, V. M. Martínez, S. Furukawa, M. Kondo, S. Shimomura, H. Uehara, M. Nakahama, K. Sugimoto and S. Kitagawa, *Nat. Commun.*, 2010, **2**, 168.
- (a) Y. Inokuma, S. Yoshioka, J. Ariyoshi, T. Arai, Y. Hitora, K. Takada, S. Matsunaga, K. Rissanen and M. Fujita, *Nature*, 2013, **495**, 461–466; (b) S. Tashiro and M. Shionoya, *Bull. Chem. Soc. Jpn.*, 2014, **87**, 643–654; (c) P. Falcaro, K. Okada, T. Hara, K. Ikgaki, Y. Tokudome, A. W. Thornton, A. J. Hill, T. Williams, C. Doonan and M. Takahashi, *Nat. Mater.*, 2016, **16**, 342–348.
- (a) H. Furukawa, K. E. Cordova, M. O’Keeffe and O. M. Yaghi, *Science*, 2013, **341**, 1230444; (b) S. Kitagawa, R. Kitaura and S. Noro, *Angew. Chem., Int. Ed.*, 2004, **43**, 2334–3275; (c) G. Férey, *Chem. Soc. Rev.*, 2008, **37**, 191–214.
- (a) R. Gaillac, P. Pullumbi, K. A. Beyer, K. W. Chapman, D. A. Keen, T. D. Bennett and F.-X. Coudert, *Nat. Mater.*, 2017, **16**, 1149–1154; (b) D. Umeyama, S. Horike, M. Inukai, T. Itakura and S. Kitagawa, *J. Am. Chem. Soc.*, 2015, **137**, 864–870; (c) T. D. Bennett, J. C. Tan, Y. Yue, E. Baxter, C. Ducati, N. J. Terrill, H. H. M. Yeung, Z. Zhou, W. Chen, S. Henke, A. K. Cheetham and G. N. Greaves, *Nat. Commun.*, 2015, **6**, 8079.
- (a) N. Giri, C. E. Davidson, G. Melaugh, M. G. Del Pópolo, J. T. A. Jones, T. Hasell, A. I. Cooper, P. N. Horton, M. B. Hursthouse and S. L. James, *Chem. Sci.*, 2012, **3**, 2153–2157; (b) N. Giri, M. G. Del Pópolo, G. Melaugh, R. L. Greenaway, K. Rätzke, T. Koschine, L. Pison, M. F. C. Gomes, A. I. Cooper and S. L. James, *Nature*, 2015, **527**, 216–220; (c) A. I. Cooper, *ACS Cent. Sci.*, 2017, **3**, 544–553.
- T. Kato, J. Uchida, T. Ichikawa and T. Sakamoto, *Angew. Chem. Int. Ed.*, 2018, **57**, 4355–4371.
- (a) M. Stępień, B. Donnio and J. L. Sessler, *Angew. Chem. Int. Ed.*, 2007, **46**, 1431–1435; (b) K. Sato, Y. Itoh and T. Aida, *J. Am. Chem. Soc.*, 2011, **133**, 13767–13769; (c) H. Norouzi-Arasi, W. Pisula, A. Mavrniskiy, X. Feng and K. Müllen, *Chem.–Asian J.*, 2011, **6**, 367–371; (d) S. Kawano, Y. Ishida and K. Tanaka, *J. Am. Chem. Soc.*, 2015, **137**, 2295–2302; (e) J. Uchida, M. Yoshio, S. Sato, H. Yokoyama, M. Fujita and T. Kato, *Angew. Chem. Int. Ed.*, 2017, **56**, 14085–14089.
- (a) K. Kishikawa, A. Hirai and S. Kohmoto, *Chem. Mater.*, 2008, **20**, 1931–1935; (b) X. Feng, M. E. Tousley, M. G. Cowan, B. R. Wiesenaus, S. Nejadi, Y. Choo, R. D. Noble, M. Elimelech, D. L. Gin and C. O. Osuji, *ACS Nano*, 2014, **8**, 11977–11986; (b) G. M. Bögers, H. P. C. van Kuringen, I. K. Shishmanova, I. K. Voets, A. P. H. J. Schenning and R. P. Sijbesma, *Adv. Mater. Interfaces*, 2015, **2**, 1500022; (c) C. Li, J. Cho, K. Yamada, D. Hashizume, F. Araoka, H. Takezoe and T. Aida and Y. Ishida, *Nat. Commun.*, 2015, **6**, 8418; (d) D. J. Mulder, L. M. W. Scheres, J. Dong, G. Portale, D. J. Broer and A. P. H. J. Schenning, *Chem. Mater.*, 2017, **29**, 6601–6605; (e) S. Bhattacharjee, J. A. M. Lugger and R. P. Sijbesma, *Macromolecules*, 2017, **50**, 2777–2783.
- (a) D. J. Tranchemontagne, Z. Ni, M. O’Keeffe and O. M. Yaghi, *Angew. Chem. Int. Ed.*, 2008, **47**, 5136–5147; (b) K. Harris, D. Fujita and M. Fujita, *Chem. Commun.*, 2013, **49**, 6703–6712; (c) N. Ahmad, A. H. Chughtai, H. A. Younus and F. Verpoort, *Coord. Chem. Rev.*, 2014, **280**, 1–27.
- (a) M. Eddaoudi, J. Kim, J. B. Wachter, H. K. Chae, M. O’Keeffe and O. M. Yaghi, *J. Am. Chem. Soc.*, 2001, **123**, 4368–4369; (b) J.-R. Li and H.-C. Zhou, *Nat. Chem.*, 2010, **2**, 893–898.
- (a) H. Furukawa, J. Kim, K. E. Plass and O. M. Yaghi, *J. Am. Chem. Soc.*, 2006, **128**, 8398–8399; (b) S. Sato, M. Ikemi, T. Kikuchi, S. Matsumura, K. Shiba and M. Fujita, *J. Am. Chem. Soc.*, 2015, **137**, 12890–12896; (c) A. V. Zhukhovitskiy, M. Zhong, E. G. Keeler, V. K. Michaelis, J. E. P. Sun, M. J. A. Hore, D. J. Pochan, R. G. Griffin, A. P. Willard and J. A. Johnson, *Nat. Chem.*, 2016, **8**, 33–41; (d) N. Hosono, M. Gochomori, R. Matsuda, H. Sato and S. Kitagawa, *J. Am. Chem. Soc.*, 2016, **138**, 6525–6531; (e) N. Hosono, K. Omoto and S. Kitagawa, *Chem. Commun.*, 2017, **53**, 8180–8183; (f) K. Omoto, N. Hosono, M. Gochomori, K. Albrecht, K. Yamamoto and S. Kitagawa, *Chem. Commun.*, 2018, **54**, 5209–5212

Metal-organic polyhedral cages with paraffinic side chains are designed as "porous modules" that self-organize into three-dimensional ordering structures and form into a self-supporting film, affording solution processable porous materials.



280x110mm (300 x 300 DPI)